Classical Force Field Parameters for the Heme Prosthetic Group of Cytochrome *c*

FELIX AUTENRIETH,[1] EMAD TAJKHORSHID,[2] JEROME BAUDRY,[1]
ZAIDA LUTHEY-SCHULTEN[1,2]
[1]*School of Chemical Sciences and* [2]*Beckman Institute, University of Illinois at Urbana–Champaign, Urbana, Illinois 61801*

Received 9 April 2004; Accepted 8 May 2004
DOI 10.1002/jcc.20079
Published online 2 July 2004 in Wiley InterScience (www.interscience.wiley.com).

Abstract: Accurate force fields are essential for describing biological systems in a molecular dynamics simulation. To analyze the docking of the small redox protein cytochrome *c* (cyt *c*) requires simulation parameters for the heme in both the reduced and oxidized states. This work presents parameters for the partial charges and geometries for the heme in both redox states with ligands appropriate to cyt *c*. The parameters are based on both protein X-ray structures and *ab initio* density functional theory (DFT) geometry optimizations at the B3LYP/6-31G* level. The simulations with the new parameter set reproduce the geometries of the X-ray structures and the interaction energies between water and heme prosthetic group obtained from B3LYP/6-31G* calculations. The parameter set developed here will provide new insights into docking processes of heme containing redox proteins.

© 2004 Wiley Periodicals, Inc. J Comput Chem 25: 1613–1622, 2004

Key words: DFT; charges; CHARMM; AMBER; Fe ligation

Introduction

The heme prosthetic group plays a central role in a variety of biological systems mediating electron transfer, oxygen transport, and apoptosis.[1–4] In the respiratory chain and bacterial photosynthesis, the small redox protein cytochrome *c* (cyt *c*) shuttles electrons between two major membrane protein complexes.[1,2] In bacterial photosynthesis, cyt *c* docks transiently at the photosynthetic reaction center, recharging it with electrons after charge separation has occurred. The oxidized cyt *c* then dissociates from the reaction center and redocks to the ubiquinone–cytochrome bc_1 complex to recover to its reduced form. In this process the heme prosthetic group changes its redox state from Fe(II) to Fe(III). To understand the docking and electron transfer process for cyt *c*, one has to describe the charge distribution on the heme prosthetic group in both redox states. The heme prosthetic group of cyt *c* is held in place through connection to four conserved amino acid side chains[5,6] shown in Figure 1a. The heme central iron is ligated to both a histidine and a methionine from the protein. Two vinyl groups of the central porphyrin ring are linked via thioether bonds to two cysteines to the protein. Over the last 2 decades cyt *c* crystal structures for both reduced and oxidized forms have become available from a variety of organisms,[7] and most recently the structures of docked cyt *c* membrane protein complexes have been solved.[8,9] Cyt *c* has essentially the same structure in all three domains of life.[2,7]

The reduced cyt c_2 high resolution structure of *Rb. sphaeroides* (PDB code: 1CXC) has been employed to initialize our quantum mechanical (QM) calculations and test the resulting parameters for the classical force fields CHARMM27[10,11] and AMBER.[12] A set of force field parameters for the unligated reduced form is available in CHARMM27[11,13] and AMBER.[12,14] In this work we primarily focus on obtaining a charge set for both redox forms as well as on developing new CHARMM parameters around the iron ligation point. An extensive vibrational study of heme is in progress by the group of MacKerell (personal communication) to fit the CHARMM force field better to vibrational normal modes obtained by infrared and resonance Raman spectroscopy on metalloporphyrin systems.[15,16] Our geometry optimizations employ density functional theory (DFT) calculations at the B3LYP level,

Correspondence to: Z. Luthey-Schulten; e-mail: zan@uiuc.edu

Contract/grant sponsor: National Institute of Health; contract/grant number: PHS2P41RR05969

Contract/grant sponsor: National Science Foundation; contract/grant number: MCB02-35144

Contract/grant Sponsor: National Resource Allocation Committee Grant

This article includes Supplementary Material available from the authors upon request or via the Internet at http://www.interscience.wiley.com/jpages/0192-8651/suppmat.

© 2004 Wiley Periodicals, Inc.

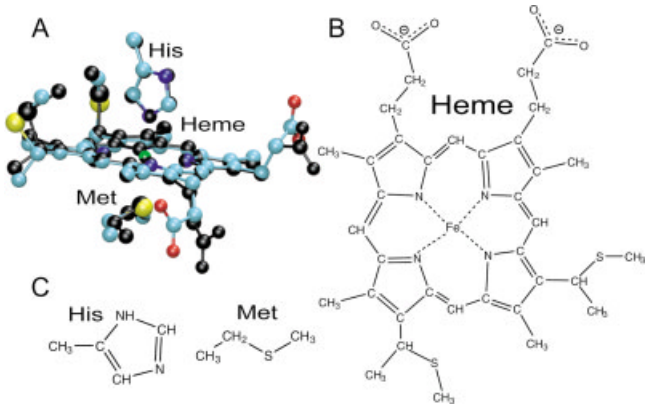

Figure 1. Chemical structure of the heme prosthetic group. (A) X-ray structure (black) superimposed upon geometry optimized structure (cyan). Connectivity of the heme (B) and ligands (C) used in the QM calculations.

which have been already successfully applied for parametrization of bacteriochlorophyll, a magnesium-porphyrin system.[17] DFT methods are widely applied to metalloproteins[18] and therefore also for modeling iron–porphyrin systems, and have been found to predict accurately nuclear magnetic resonance shifts[19] as well as binding energies for the iron–sulfur bond.[20] The original charge calculations for both CHARMM and AMBER force fields were done at the HF/6-31G* level for small chemical compounds.[10–12] As the heme prosthetic group cannot be divided into smaller chemical compounds without losing the biological relevance of the system, we chose to use B3LYP/6-31G* for all final calculations for the CHARMM force field. Our QM geometries have been compared to high resolution structures from eight different organisms as well as to previous DFT calculations on iron–porphyrin systems.[20]

It has been found that the current CHARMM27 parameters for the central reduced heme porphyrin system without ligands could represent the geometries obtained by QM calculations but are in partial disagreement with spectroscopic data.[15,16] The missing parameters around the iron–ligand attachment points cannot be easily inferred from other CHARMM parameters, and had to be fitted either to geometries obtained by our DFT calculations or to experimentally determined spectra of heme.[15,16] We calculated and compared charges for the two redox states by both DFT and Hartree–Fock (HF) calculations. The Mulliken charges obtained by DFT calculations were scaled following closely the CHARMM parameter development scheme.[11] The electrostatic potential (ESP) charges obtained by HF calculations were scaled according to the restrained ESP (RESP) methodology[21] widely applied in AMBER.[12] *Ab initio* charge distributions for both redox forms have been obtained by an LCAO SCF MO calculation using a double zeta basis set by Kashiwagi et al.[22] and compared to our results. The final charge differences between the oxidized and reduced forms implemented with CHARMM indicate a clear change in the electrostatic potential at the surface of cyt *c*. The new charges and parameters will provide more accurate simulations for understanding heme proteins, and will extend the usability of the common force fields CHARMM and AMBER.

Computational Methods

Parameter development for empirical force fields such as CHARMM[10] and AMBER[12] is accelerated by the modular character of these force fields. Following standardized protocols based on the original development of these force fields ensures the transferability of parameters for new chemical compounds.

Form of the Force Fields

The functional form of the CHARMM potential function is given in eq. (1). The energy function comprises the following bonded interactions: bond stretch and bond angle terms, 1,3 Urey–Bradley coupling terms, sinusoidal dihedral and harmonic improper dihedral terms. The symbols r, θ, ϕ, φ, and $r_{1,3}$ represent the bond lengths, bond angles, dihedral angles, improper angles, and Urey–Bradley distances for any given conformation of the molecule, r_{eq}, θ_{eq}, ϕ_{eq}, φ_{eq}, and $r_{1,3,eq}$ are the equilibrium values for these properties, and the associated force constants are k_r, k_θ, k_ϕ, k_φ and k_{UB}. In the dihedral term n represents the multiplicity of the rotor (e.g., three for a methyl group) and δ is the phase angle. Nonbonded interactions between pairs of atoms (i, j) are described by the Coulomb and van der Waals (VDW) potentials, respectively. The atom pairs are separated by at least three bonds, and the VDW energy is calculated by a Lennard–Jones potential with a well depth ε, position of the minimum R_{min}, and distance $r_{i,j}$. The electrostatic energy between partial charges q_i and q_j separated by r_{ij} is described by a Coulomb potential. ε is the dielectric constant of the protein/medium. The functional form of the AMBER potential function is given in eq. (2). The form of the energy function is almost identical to CHARMM, the major difference being the omission of the Urey–Bradley terms. Although functionally similar the strategy to assign partial charges is quite different.

$$E_{\mathrm{CHARMM}} = \sum_{\text{bonds}} K_r(r - r_{eq})^2 + \sum_{\text{angles}} K_\theta(\theta - \theta_{eq})^2 + \sum_{\text{dihedrals}} K_\phi[1 + \cos(n\phi - \delta)] + \sum_{\text{impropers}} K_\varphi(\varphi - \varphi_{eq})^2 + \sum_{\text{Urey-Bradley}} K_{UB}(r_{1,3} - r_{1,3eq})^2 + \sum_{\text{electrostatics}} \frac{q_i q_j}{r_{ij}\varepsilon} + \sum_{\text{VDW}} \varepsilon_{ij}\left[\left(\frac{R_{\min,ij}}{r_{ij}}\right)^{12} - 2\left(\frac{R_{\min,ij}}{r_{ij}}\right)^{6}\right] \quad (1)$$

$$E_{\mathrm{AMBER}} = \sum_{\text{bonds}} K_r(r - r_{eq})^2 + \sum_{\text{angles}} K_\theta(\theta - \theta_{eq})^2 + \sum_{\text{dihedrals}} \frac{V_n}{2}[1 + \cos(n\phi - \gamma)] + \sum_{\text{nonbonded}} \left\{4\varepsilon_{ij}\left[\left(\frac{R_{\min,ij}}{r_{ij}}\right)^{12} - 2\left(\frac{R_{\min,ij}}{r_{ij}}\right)^{6}\right] + \left[\frac{q_i q_j}{r_{ij}\varepsilon}\right]\right\} \quad (2)$$

Systems and Geometries

The chemical structure of the heme prosthetic group is depicted in Figure 1. The prosthetic group of cyt *c* consists of a heme, one iron-ligated histidine, and one iron ligated methionine, as well as two cysteine residues covalently connected through thioether link-

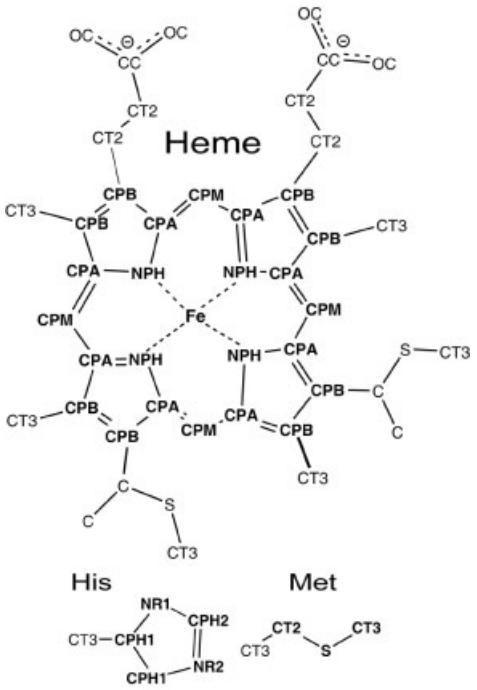

Figure 2. CHARMM atom types for the heme prosthetic group. The parts depicted in bold have been subjected to B3LYP/6-31G* geometry optimizations and are referred to as core structure. The attached side chains have been geometry optimized by HF/STO-3G keeping the core fixed. The parameters in Table 2 and 3 are given in terms of atom types defined here.

ages to the heme. The amino acid backbone atoms of the ligating histidine and methionine have been omitted in the QM calculations. B3LYP/6-31G* geometry optimizations with no constraints were performed on a truncated system that is comprised of the central iron–porphyrin macrocyle with the ligands imidazole and dimethyl-sulfide (DMS), representing histidine and methionine, respectively. This system without any side chains will be referred to as the *core* in the following text. The atoms of the core system are depicted in bold in Figure 2. The omitted side chains are the four methyl, two proprionate, and two ethylthioethermethyl groups connected to the iron–porphyrin macrocyle as well as two methyl groups connected to imidazole and DMS, respectively. All atoms in Figure 2 are depicted with their respective CHARMM atom types used in the tables and the text. The charges states and multiplicities for the individual redox states are summarized in Table 1.

All initial structures were taken from the high-resolution X-ray structure of cyt *c* from *Rb. sphaeroides* (PDB accession code 1CXC).[5] Hydrogen atoms were added with the package Spartan.[23] *Ab initio* DFT geometry optimizations at the B3LYP/6-31G* level were performed in Gaussian03[24] on the core structures for both redox states. The side chains were subsequently attached to the optimized core structures, and the distances of the bonds linking the side chains to the core were manually adjusted to the X-ray structure using Spartan.[23] Subsequently, all hydrogens were minimized in Spartan[23] keeping the geometry of all heavy atoms fixed. The side chains of heme were geometry optimized with HF/STO-3G in Gaussian03.[24] The geometries of the core structures obtained at a higher level of theory were fixed during side chain optimization. The optimized geometries were compared to seven X-ray structures with the following PDB accession codes: 1YTC, 1CXC, 1C2R, 1HRO, 1IO3, 3C2C, 1QN2, and 5CYT. Visualization and geometry analysis were performed with the program VMD.[25]

Equilibrium distances (R_{eq}) derived from the QM geometry optimization were introduced only when the bond deviations between the original CHARMM27 force field and the QM structure were larger than 0.05 Å. This was the case only around the iron-ligation points. The missing bond length of the iron–sulfur bond was adjusted manually to reproduce the *ab initio* calculated geometries. The normal mode contributions of the core heme prosthetic group generated by the Vibran facility included in the CHARMM package[10] were compared to available spectroscopic data, and the equilibrium values and force constants of the Fe—S and Fe—NR2 bonds were adjusted accordingly. The geometric parametrization carried out for the iron-ligation points will be discussed in detail in the Results section.

Rotational barriers around the Fe—S and Fe—NR2 bonds in the core of the reduced (FeII) system were investigated using Spartan[23] at the B3LYP/6-31G* level of theory, starting from the B3LYP/6-31G* optimized system and freezing the heme's atomic coordinates in the plane. The dihedral force constants in the force field were adjusted to reproduce the *ab initio* values calculated by Spartan.[23] The heme–cysteine linkages as well as missing angle parameters for the methionine iron linkage were modeled by analogy to the CHARMM parametrized residue methionine.

Charge Fitting for the CHARMM Force Field

Mulliken charges on the heme prosthetic group were obtained by Gaussian03[24] from both HF/6-31G* and B3LYP/6-31G*. Mulliken charges, calculated for two different side-chain conformations, were found to be conformation independent. To incorporate the partial charges into the force field according to the CHARMM

Table 1. Charges and Multiplicities.

System	Charge	Multiplicity	Description
Fe(II)P-Im-DMS	0	Singlet	core reduced
Fe(III)P-Im-DMS	+1	Doublet	core oxidized
Heme(II)-His-Met-2Cys	−2	Singlet	heme prosthetic reduced
Heme(III)-His-Met-2Cys	−1	Doublet	heme prosthetic oxidized

Table 2. Bond Distance (Å), Angle (Degrees), and Dihedral (Degrees) Values for the Reduced Heme Core Structures after Geometry Optimization (B3LYP/6-31G*).

Parameters	Optimized QM	1CXC	1YTC	Mean X-ray[a]	CHARMM	Rovira
Bonds						
FE-NPH	2.01	1.97	2.01	2.00 ± 0.05	1.96 (1.93)[b]	2.00
NPH-CPA	1.38	1.39	1.38	1.38 ± 0.02	1.36	1.39
CPA-CPB	1.45	1.45	1.46	1.43 ± 0.05	1.46	1.44
CPB-CPB	1.36	1.35	1.34	1.36 ± 0.05	1.36	1.37
CPB-CPM	1.39	1.38	1.37	1.37 ± 0.02	1.36	1.39
NR2-CPH1	1.38	1.41	1.36	1.38 ± 0.04	1.39	1.33
CPH1-CPH1	1.37	1.38	1.38	1.38 ± 0.04	1.35	1.36
NR1-CPH1	1.38	1.40	1.37	1.38 ± 0.03	1.37	1.38
NR1-CPH2	1.36	1.35	1.35	1.33 ± 0.03	1.36	1.37
CPH2-NR2	1.32	1.30	1.33	1.32 ± 0.03	1.31	1.39
S-CT3	1.82	1.82	1.82	1.82 ± 0.01	1.83	1.82
NR2-FE	1.99	2.02	2.04	2.03 ± 0.15	1.95 (2.12)[b]	2.04
S-FE	2.44	2.36	2.37	2.31 ± 0.18	2.50	2.23
Angles						
CPB-CPM-CPB	125	125	127	126 ± 1	127	125
NPH-FE-NPH(1)	90	90	91	90 ± 0	90	90
NPH-FE-NPH(2)	179	179	179	178 ± 2	170	177
CPH2-NR2-CPH1	106	109	110	108 ± 3	105	106
CPH1-CPH1-NR2	110	104	108	107 ± 3	111	110
NR2-CPH2-NR1	110	113	107	110 ± 3	112	110
NPH-FE-S	92	91	90	90 ± 2	95	89
NPH-FE-NR2	90	90	90	90 ± 2	85	88
NR2-FE-S	175	178	172	175 ± 9	178	177
CT3-S-CT3	99	99	98	99 ± 5	94	98
Dihedrals						
NPH-FE-S-CT3	−11	−35	−31	−37 ± 4	−33	176
NPH-FE-NR2-CPH2	44	51	48	47 ± 4	46	−9

The values are compared to X-ray structures and B3LYP/6-31G* calculations carried out by Rovira et al.[20]
[a]Average variations observed in seven high resolution X-ray structures from all domains of life, which included the systems 1CXC (*Rb. sphaeroides*) and 1YTC (*S. cerevisiae*) in direct comparison.
[b]Values in brackets are obtained after minimization with original equilibrium distances provided by CHARMM27.[10,11]

parametrization protocol,[11] the charges at all nonpolar hydrogens of the heme prosthetic group have been set to a value of 0.09 e and the excessive positive charge added into the adjacent carbon atoms. Charges on equivalent atom types were averaged, and finally the charges on the four polar side groups were adjusted to reproduce the quantum mechanically obtained interaction energies of the reduced heme with water. Interaction energies have been only calculated for the B3LYP/6-31G* Mulliken charges, which were employed in the final simulations. The CHARMM force field is optimized for molecular dynamics simulations with the TIP3P water model.[26] Therefore, water-solute interactions are of major importance, and it is necessary to scale the charges of the solute in the force field to reproduce the quantum mechanically obtained interaction energies. For this purpose, four independent water molecules were placed within hydrogen-bond distance of the polar side chains of the heme prosthetic group. The initial water positions were geometry optimized with fixed heme geometries using the semiempirical PM3[27] method in Spartan.[23] Interaction energies between an individual water molecule and the system were calculated with B3LYP/6-31G* as the difference between the energies of the heme–water complex and the sum of the individual monomers (water and heme prosthetic group separated).

B3LYP/6-31G* interaction energy calculations were applied in the same way for the oxidized form. The scaling factor with one water molecule near proprionate was 0.15 and was the same for reduced and oxidized forms. The factor was determined from the relative difference between quantum mechanically derived and scaled Mulliken charges. As can be seen in Table 5, the difference in interaction energies between CHARMM and B3LYP/6-31G* for the scaled oxidized charges deviated only by 1.12 kcal/mol for Wat3. Therefore, this factor was applied for the remaining proprionic side groups in the oxidized form.

To estimate how well the CHARMM parameters reproduce the total interaction energy of the four waters, we compare the B3LYP/6-31G* and the CHARMM values when all four waters were simultaneously removed. As there is little interaction between the waters, the total interaction energies differ only by 1.2 kcal/mol. In comparison, the sum of the individual water-solute interaction energies shown in Table 5 is −69.32 kcal/mol for the CHARMM and −68.88 kcal/mol for the B3LYP/6-31G*

Table 3. Bond Distance (Å), Angle (Degrees), and Dihedral (Degrees) Values for the Oxidized Heme Core Structures after Geometry Optimization (B3LYP/6-31G*).

Parameters	Optimized QM	2YCC[a]	CHARMM	Rovira
Bonds				
FE-NPH	2.00	2.01	1.95 (1.93)[b]	2.01
NPH-CPA	1.38	1.38	1.36	1.39
CPA-CPB	1.44	1.46	1.46	1.44
CPB-CPB	1.36	1.33	1.36	1.37
CPB-CPM	1.39	1.38	1.36	1.39
NR2-CPH1	1.38	1.39	1.39	1.33
CPH1-CPH1	1.36	1.37	1.35	1.35
NR1-CPH1	1.38	1.35	1.37	1.38
NR1-CPH2	1.35	1.33	1.36	1.37
CPH2-NR2	1.33	1.36	1.31	1.39
S-CT3	1.82	1.84	1.83	1.81
NR2-FE	1.97	2.01	1.95 (2.06)[b]	2.04
S-FE	2.47	2.43	2.50	2.27
Angles				
CPB-CPM-CPB	125	126	127	125
NPH-FE-NPH(1)	90	90	90	90
NPH-FE-NPH(2)	177	176	170	179
CPH2-NR2-CPH1	107	104	105	107
CPH1-CPH1-NR2	109	111	111	110
NR2-CPH2-NR1	110	110	112	109
NPH-FE-S	89	90	95	86
NPH-FE-NR2	91	90	85	89
NR2-FE-S	174	170	179	174
CT3-S-CT3	100	94	94	99
Dihedrals				
NPH-FE-S-CT3	−10	−36	−33	173
NPH-FE-NR2-CPH2	46	65	43	−14

The values are compared to X-ray structures and B3LYP/6-31G* calculations carried out by Rovira et al.[20].

[a]Direct comparison to high-resolution structure 2YCC (*S. cerevisiae*).

[b]Values in brackets are obtained after minimization with original equilibrium distances provided by CHARMM27.[10,11]

calculations, respectively yielding a difference in overall interaction energies of only 0.44 kcal/mol. It was not necessary to move the individual water molecules to various positions around the side groups, as VDW parameters were not adjusted. The original CHARMM VDW parameters have been kept for all atoms.

Charge Fitting for the AMBER Force Field

The electrostatic potential (ESP) obtained from HF/6-31G* wave functions of the heme prosthetic group with Gaussian03.[24] The charges derived from this potential (ESP charges) were calculated employing the Merz–Kollman scheme.[28] Restricted ESP (RESP) charges[21] were obtained by imposing symmetry on the hydrogens and by constraining the charge on the central iron. It optimally reproduces the intermolecular interactions without surrounding solvent molecules. This fitting protocol is used for AMBER parameter development.[12] The applied constraints used in the RESP calculation are discussed in the results section.

Minimization and Molecular Dynamics

Minimizations of the heme prosthetic group *in vacuo* as well as in solvated cyt *c* were performed employing the newly developed set of parameters. All structures were minimized for 10,000 steps in NAMD2[29] using our modified version of the CHARMM force field.[11]

Cyt *c* was solvated in a box of water using the program Solvate included in the NAMD2 package.[29] The system was minimized for 10,000 steps and equilibrated for 1 ns under NPT ensemble conditions with full electrostatics calculated using the Particle–Mesh Ewald approach.

Electrostatic Potential Analysis

Electrostatic potential calculations for the final charge sets of the heme prosthetic group inside cyt *c* were carried out with DelPhi,[30] which solves the nonlinear Poisson–Boltzman equation. The newly developed charge sets for the heme prosthetic group as well as the standard CHARMM charge set for the rest of the protein were

employed. For the calculation of the electrostatic potential map an internal dielectric constant of 4 and an external dielectric constant of 80 were employed. The grid spacing was 2 grids/Å. The electrostatic potential map was visualized with GRASP.[31]

Results and Discussion

Geometries

The results of the *ab initio* B3LYP/6-31G* geometry optimization of the reduced and oxidized heme prosthetic group are summarized in Tables 2 and 3, respectively. CHARMM atom types are defined in Figure 2. In Table 2, the comparisons are to the X-ray structures of two reduced cyt *c* proteins, *Rb. sphaeroides* (PDB accession code 1CXC), used to initialize the geometry optimization as well as to the high-resolution X-ray structure of cyt *c* from *Saccharomyces cerevisiae,* which is available in both redox states. The X-ray geometries of all eight X-ray structures agree well with our *ab initio* optimized geometries, especially in the core structure. The bond mean values deviate between the eight X-ray structures by less than 0.05 Å for the porphyrin macrocycle and the ligands. The bond values obtained by both B3LYP/6-31G* geometry optimization and CHARMM minimization are well within that range. The only bonds with significant deviations from the X-ray structures are the iron–sulfur (Fe—S) and iron–histidine (Fe—NR2) bonds. The standard deviations of the Fe—S and Fe—NR2 bonds in the eight X-ray structures are 0.18 and 0.15 Å, respectively.

Table 3 compares the *ab initio* optimized geometry of the oxidized heme prosthetic group to the high resolution X-ray structure of cyt *c* from *S. cerevisiae* in the oxidized state. As there are not many high-resolution X-ray structures available for cyt *c*, in the oxidized state only this structure was employed for comparison. The geometric difference between the reduced and oxidized structures of yeast cyt *c* available in both redox states is less than 0.01 Å in the porphyrin macrocyle and only slightly higher for the iron ligands. Due to these small geometric differences in both QM calculations and X-ray structures our newly introduced CHARMM parameters use the same bonded equilibrium values and force constants for both redox forms, and differ only with respect to partial atomic charges.

Tables 2 and 3 also compare our results with the DFT calculations of Rovira et al.[20] While the iron–sulfur bond distance obtained by our DFT calculations is 0.2 Å larger than the one reported by Rovira et al., both results are within the variation of bond distances observed in the X-ray structures. The iron–sulfur bond difference of 0.04 Å between the two redox states could be reproduced by our *ab initio* geometry optimization.

Tables 2 and 3 also report the geometries after minimization with our newly developed CHARMM force field parameters. The added bond length and dihedral parameters will be discussed in detail in the "iron ligand parameters" section. Extensive calculations on the bonded interactions are being performed by the group of MacKerell on the macrocycle in order to better fit force constants to vibrational data (personal communication). It has been found that the geometries of the X-ray structures and QM calculations around the iron-ligation points could not be reproduced well by the original equilibrium distances provided by CHARMM.[10,11] The values obtained by minimization with the original CHARMM force field are depicted in brackets in Tables 2 and 3. We could improve the geometries slightly by employing the distances obtained in our DFT/B3LYP geometry optimization of the core heme prosthetic group.

Table 4. Deviation from Planarity (Degrees).

PDB code	Angle CPM-FE-CPM
B3LYP/6-31G* Oxidized	174
B3LYP/6-31G* Reduced	177
2YCC (*S. cerevisiae* oxidized)	165
1YTC (*S. cerevisiae* reduced)	171
Rovira oxidized	176
Rovira reduced	179
1CXC	176
1C2R	179
1HRO	177
1IO3	174
3C2C	176
1QN2	169
5CYT	173

It is well known that the heme group in X-ray structures is not absolutely planar, and is distorted into a slightly bent structure.[7] The deviation from planarity of several high-resolution X-ray structures as well as the *ab initio* geometry optimized structures is summarized in Table 4. The deviation from planarity measured as the angle of two oppositely lying CPM atoms and the central iron can be as large as 11 degrees in the case of *Methylobacterium extorquens*[32] (PDB accession code 1QN2). DFT calculations on porphyrin systems[17,20] and X-ray structures from *S. cerevisiae* (PDB accession codes 1YTC and 2YCC)[33] show that the reduced heme group is more planar compared to the oxidized form. This result is in full accord with the results of our calculations, in which the optimized structures of the two redox states differ from each other by three degrees even though we started both geometry optimizations from the same starting structure taken from X-ray structure of *Rb. sphaeroides.*

The side-chain conformations obtained by HF/STO3G geometry optimizations exhibit significant deviations from the X-ray structures as they can undergo torsional rotations of several degrees (see Fig. 1). These side-chains rotations are only observed for *in vacuo* calculations as the heme is tightly bound inside cyt *c*.

Charge Distribution of Heme in Reduced and Oxidized Forms

Initial Mulliken charges have been obtained for the core and for the complete heme prosthetic group. For the complete heme prosthetic group Mulliken charges have been scaled in a CHARMM consistent manner by calculating interaction energies between individual water molecules placed near the four polar side groups (proprionic acids and cysteine linkages). The energy difference between QM and CHARMM27 is below 1 kT (0.6 kcal/mol) for the four water molecules (Table 5). The final scaled charge sets obtained by DFT/B3LYP for the core structures and the complete

Table 5. Water–Solute Interaction Energies for the Reduced Form (kcal/mol).

	CHARMM	B3LYP/6-31G*	Difference
Wat1(Cys15)	−4.50	−4.93	−0.43
Wat2(O1A, O2A)	−37.83	−37.71	0.12
Wat3(O1D, O2D)	−21.58	−20.91	0.67
Wat4(Cys18)	−5.41	−5.33	0.08
Wat3(oxidized)	−19.81	−20.93	1.12

heme prosthetic groups are summarized in Figures 3 and 4, respectively.

Comparison of the oxidized and reduced core structures depicted in Figure 3 reveals the following features. The porphyrin macrocycle transfers ionic charge onto the central iron. Iron carries a partial charge of +1.21 e in the reduced form, and +1.33 e in the oxidized form, charges that are smaller than the formal oxidation states for the reduced (+II) and oxidized (+III) forms. The excess positive charge is distributed over the whole porphyrin system. This transfer can be readily explained by examining the heme biosynthetic pathway.[2] Two central polar porphyrin hydrogens are replaced by the ferrous form of iron generating a neutral reduced iron–porphyrin system. The charge distribution in the core structures is highly symmetric, and identical atom types exhibit the same charge, even before averaging or scaling of charges. Interestingly the excess of the positive charge is transferred mainly to the periphery of the molecule. The extent of the charge transfer onto the periphery of the molecule is also the major difference between oxidized and reduced form. With exception of the central iron only the charges on atoms that are nonburied, and lie on the periphery show significant changes after oxidation. The difference between the two redox states is as large as 0.07 e for all carbons, which are connected to side groups in the complete heme prosthetic group. The charges on the buried porphyrin nitrogens differ only by 0.03 e between the oxidized and reduced forms, and the adjacent carbon atoms are identical with a charge of 0.34 e in both redox states. The charges on the imidazole and DMS ligands vary around 0.05 e between the two redox states on identical atoms.

As shown in Figure 4, the tendency of charge transfer onto the periphery of the molecule is also apparent in the complete heme prosthetic group. The central iron–porphyrin charges are almost identical compared to the calculations on the core structures, whereas charges on the side groups differ significantly between the two redox states. The largest deviation between the reduced and oxidized forms can be found on the proprionic acid groups, where the two redox states differ from each other by as much as 0.1 e on individual atoms. Therefore, the focus in modeling the difference between both redox states was on scaling the side group charges to reproduce interaction energies in CHARMM. The charge difference on the heme proprionic side groups could not have been reproduced by modeling the charges in analogy to glutamic acid. Our approach allowed us to model into CHARMM the different electrostatic properties observed by quantum mechanics for both redox states.

An *ab initio* LCAO self-consistent field (SCF) molecular orbital calculation was performed on a planar Fe–porphyrin systems with a double zeta basis set by Kashiwagi et al.[22] SCF wave functions of several reduced and oxidized forms of Fe–porphyrin were obtained. Total energies, electron distributions, and electron density differences between the states have been determined. The most important result of the study was that after ionization of the reduced form a considerable amount of charge flows into the central iron from the porphyrin macrocycle. The change in the net charge on iron is only 0.33 e. Therefore, the porphyrin macrocycle acts as an electron buffer and distributes the charge loss of one electron over the whole system. This result is in qualitative agreement with our *ab initio* B3LYP/6-31G* calculation where we observe a charge difference of 0.12 e between both redox states in the core system. The central iron reduces its positive charge by transferring it onto the ligands. Charge transfer after oxidation into the central iron from the porphyrin macrocycle is even larger for *ab initio* B3LYP/6-31G* calculations compared to Kashiwagi et al.[22]

The effect of these different electrostatic properties to the protein environment is shown in Figure 5, were the electrostatic potential for both charge sets is shown on the cyt *c* surface. Cyt *c* is oriented towards its docking surface, and resembles the view as it is seen by docking partners such as the photosynthetic reaction center. The heme prosthetic group is embedded into the cyt *c* structure, and only the heme edge is exposed to the docking interface. It can be seen in Figure 5 that oxidized cyt *c* has a stronger positive potential compared to the reduced cyt *c* on the docking surface. The change in electrostatic potential at the docking interface could be sensed by docking partners of cyt *c* and might lead to facilitated association or dissociation depending on the redox state.

The distribution of charge over the whole heme prosthetic group could be better reproduced by DFT/B3LYP calculations compared to HF, as DFT allows better modeling of correlation and exchange effects.[17] The Mulliken charges obtained by HF are very localized, and the major charge difference between the redox states

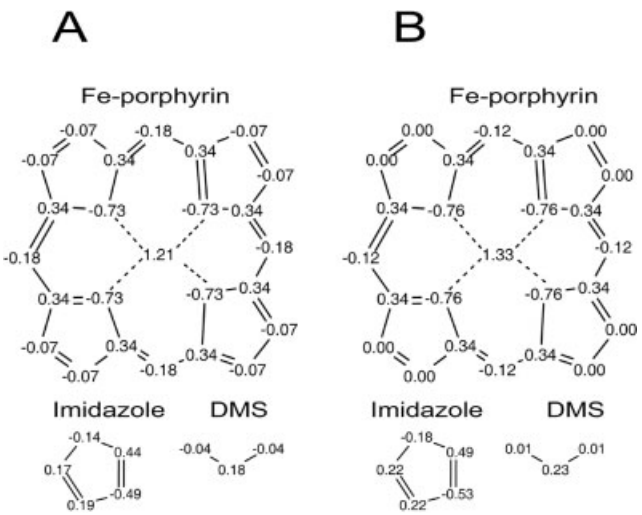

Figure 3. Unscaled Mulliken charges of the truncated core in the reduced (A) and oxidized (B) forms. Hydrogen atom charges are omitted for clarity and added into the heavy atoms.

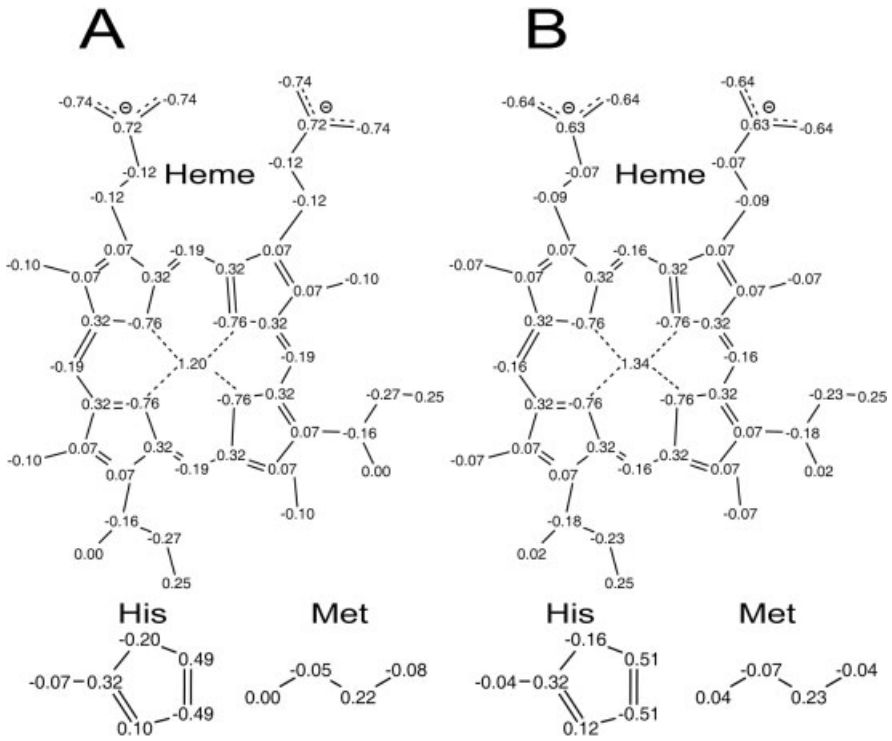

Figure 4. Scaled Mulliken charges of the heme prosthetic group in the reduced (A) and oxidized (B) forms. Hydrogen atom charges are omitted for clarity and added into the heavy atoms.

are found in the central core. The periphery exhibits no significant differences between the reduced and the oxidized forms, and the different overall charge is distributed uniformly over the whole heme prosthetic group. The unscaled HF Mulliken charges are provided in the Supplementary Materials.

Iron Ligand Parameters

To model a six-coordinated heme system several new CHARMM parameters had to be introduced at the iron ligation points. The new parameter set reproduces the geometries for both redox states in good agreement with QM calculations. Subsequent simulations of cyt *c* in an NPT ensemble for 1 ns provided a stable cyt *c* system with a backbone RMSD of 1.2 Å. A backbone RMSD value of 1.5

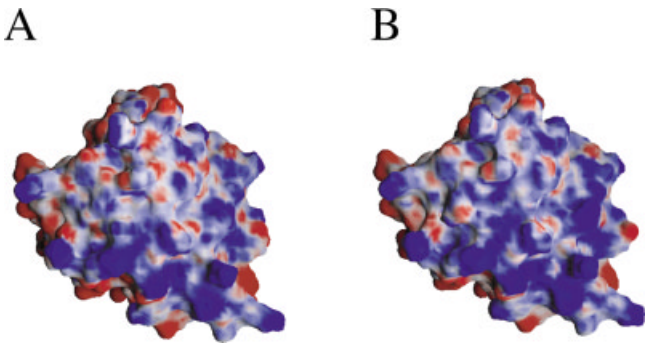

Figure 5. DelPhi generated electrostatic potential plotted on cyt *c* docking surface in the reduced (A) and oxidized (B) forms. Color code electrostatic potential: +1 blue; 0 green; −1 red. Electrostatic potential is greater on the docking surface of the oxidized form.

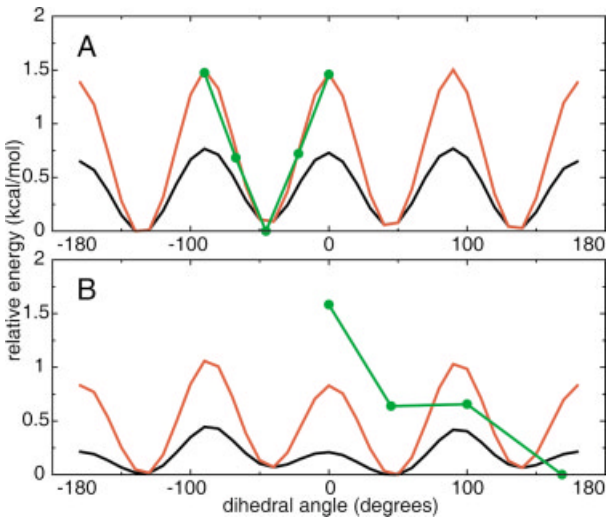

Figure 6. Energy profiles for rotation about FE-NR2 (A) and FE-S (B) bonds. Red: Calculation with new CHARMM parameters given in Table 7. Black: calculation with the dihedral force constant K_ϕ. Green: *Ab initio* calculation B3LYP/6-31G*.

Å was reported for cyt *c* simulations in the NVT ensemble using the original CHARMM parameters[34] and appropriate modifications on the Fe—S bond. The rmsd of the heme prosthetic group compared to the X-ray structure was 0.7 Å for both redox forms. The newly developed bond and dihedral parameters are summarized in Tables 6 and 7, respectively.

Fe Ligation

Despite otherwise excellent agreement with the *ab initio* geometries, the original CHARMM exhibited bond deviations of 0.08 and 0.13 Å at the porphyrin iron–nitrogen (Fe—NPH) ligation and the histidine iron–nitrogen ligation (Fe—NR2), respectively, compared to the values obtained by QM calculations (see Table 2). In addition, several parameters such as the iron–sulfur (Fe—S) and two dihedral and one improper angles defining the position of the ligands relative to heme have been missing in the CHARMM forcefield. Comparison of the CHARMM force constants of heme with force constants determined by vibrational spectra[15] revealed larger bending and stretching force constants for the metalloporphyrin spectra. To fit the CHARMM force field better to experimental spectroscopic data for metalloporphyrins extensive vibrational analysis is underway by the group of MacKerell et al. (personal communication).

The equilibrium values for Fe—NPH and Fe—NR2 were changed from 1.96 to 2.00 Å and from 2.20 to 2.00 Å, respectively, but the CHARMM force constants were unchanged. It has been found that Fe—NR2 bond stretch contributions to the normal modes obtained from these values are in good agreement with most recently determined normal modes of an iron porphyrin–imidazole compound.[16] The normal mode analysis with the new Fe—NR2 bond distance of 2.00 Å provided major energy contributions of 34% at 193 cm^{-1}. The iron–imidazole stretching mode was observed at 226 cm^{-1} with a major energy contribution of 35% for (Fe—NR2).[16] As the analysis was performed only for the truncated system the effects of ligation of heme in cyt *c* via two cysteine linkages was not taken into account. As there are four ligation points, heme is more tightly bound inside cyt *c* compared to myoglobin. One of our goals is to provide highly transferable parameters for the new geometries at the iron ligation point; therefore, only slight modifications of the original CHARMM force field for the rest of the system were introduced.

As there was no experimental data for the iron–methionine stretching mode available the force constant of the iron–sulfur bond (Fe—S) was chosen according to other observed force constants in the porphyrin macrocycle. With a force constant of 300 kcal mol^{-1} $Å^{-2}$ the QM value of 2.45 Å could be reproduced with CHARMM within 0.05 Å.

Table 6. New Bond Parameters.

Bond	CHARMM initial (Å)	CHARMM new (Å)	Force constant [kcal mol^{-1} $Å^{-2}$]
FE-NPH	1.96	2.00	270.2
FE-NR2	2.20	2.00	65.0
FE-S	—	2.45	300.0

Table 7. New Dihedral and Improper Parameters.

Dihedral[a]	Force constant[b]	Periodicity[c]	Phaseshift[d]
NPH-FE-NR2-CPH1	0.047	4	0.0
NPH-FE-NR2-CPH2	0.047	4	0.0
NPH-FE-S-CT3	0.040	4	0.0
NPH-FE-S-CT2	0.040	4	0.0
NR2-CPH1-CPH2-FE	29.4[e]	0	0.0

[a]CHARMM atom types.
[b]kcal/mol.
[c]Periodicity of torsion.
[d]Phase offset in degrees.
[e]kcal/mol/rad^2.

Ligand Dihedrals and Impropers

Figure 6 shows dihedral barriers calculated for rotations around the Fe—NR2 and Fe—S dihedrals shown in Table 7. *Ab initio* barriers were calculated at the B3LYP/6-31G* level for the Fe—S dihedral, allowing the $S(CH_3)_2$ moiety to relax while fixing the rest of the reduced core structure at its B3LYP/6-31G* optimized geometry. The Fe—NR2 barrier was calculated at the same level of theory in a rigid way. *Ab initio* calculations (green points on Figure 6) indicate a total barrier of 1.5 kcal/mol for both dihedral rotations around Fe—NR2 and Fe—S bonds. The shapes of the calculated potential energy curves differ though. The *ab initio* energy curve for the Fe—NR2 barrier is compatible with a fourfold symmetry with extrema that are in phase with the 0.6 kcal/mol barrier originating from the nonbonded interaction calculated using a dihedral force constant $k = 0$ kcal/mol (black line). The *ab initio* barrier can be reproduced by using an intrinsic dihedral term of periodicity $n = 4$ in CHARMM, distributed equally over all eight dihedrals that define the Fe—NR2 rotation (see Table 7), for an intrinsic dihedral contribution of 0.752 kcal/mol.

Initially, the imidazole ligand was not oriented with a 90-degree angle towards the porphyrin plane after minimization as observed in the QM and X-ray geometries. Therefore, the missing improper NR2—CPH1—CPH2—Fe was introduced into CHARMM and proper orientation was achieved. The force constant was chosen according to existing CHARMM force constants for iron–porphyrin systems.

The *ab initio* potential energy curve calculated for the Fe—S rotation does not exhibit a fourfold symmetry, while the nonbonded contribution to the CHARMM barrier (in black in Fig. 6) shows a fourfold symmetry with a barrier height of 0.5 kcal/mol. An intrinsic dihedral term as given in Table 7 was added to increase the total dihedral barrier to a value closer to the 1.5 kcal/mol *ab initio* barrier.

RESP Charges

For simulation with the AMBER force field RESP charges of the heme prosthetic group are needed for both redox states. It is well known that ESP charges of buried groups tend to be less well determined compared to ESP charges of peripheral groups, which

are more solvent accessible.[21] To obtain a consistent charge distribution on the heme prosthetic group, the iron atom was constrained to its Mulliken charge value and the ESP charges on adjacent porphyrin nitrogens were adjusted to conserve the overall charge. After this adjustment and forcing symmetry on equivalent atom types within the heme core, RESP charges for both redox forms were obtained. The RESP charges exhibit the same trends as the HF Mulliken charges. Differences between the two redox states are uniformly distributed over the heme prosthetic group. The RESP charges are summarized in the Supplementary Material.

Supplementary Material

1. CHARMM parameter files: cyt-new-par.inp is summary of all newly introduced parameters in CHARMM27 format.
2. CHARMM topology files: cyt-new-top.inp is summary of all newly introduced topologies in CHARMM27 format.
3. RESP charges summary RESP-charge.pdf. All hydrogens are added into heavy atoms.
4. HF generated Mulliken charges summary HF-MUL-charge.pdf. All hydrogens are added into heavy atoms. The side chains are not scaled with water molecules.

Conclusions

Our parameters provide a new set of force field parameters for the cyt *c* heme, to be used in classical simulations in both redox states. The emphasis in our study was on the charges that change significantly during the oxidation process. The new parameters describe the biological significant charge distributions over the heme prosthetic group observed by QM calculations. The significant localization of the positive charge of heme on peripheral atoms upon oxidation suggests strong implications in the interactions between heme proteins and corresponding docking partners.

Acknowledgment

We would like to thank Alexander Mackerell for helpful discussions.

References

1. Hu, X.; Ritz, T.; Damjanović, A.; Autenrieth, F.; Schulten, K. Q Rev Biophys 2002, 35, 1.
2. Berg, J.; Tymoczko, J.; Stryer, L. Biochemistry; W. H. Freeman and Company: New York, 2002.
3. Gray, H. B. Proc Natl Acad Sci USA 2003, 100, 3563.
4. Shi, Y. Nat Struct Biol 2001, 8, 394.
5. Axelrod, H. L.; Feher, G.; Allen, J. P.; Chirino, A. J.; Day, M. W.; Hsu, B. T.; Rees, D. C. Acta Crystallogr D 1994, 50, 596.
6. Salemme, F. R. Annu Rev Biochem 1977, 46, 299.
7. Scott, R. A. Cytochrome *c*: A Multidisciplinary Approach; Mauk, A. G., Eds.; University Science Books: Sausalito, CA, 1996.
8. Axelrod, H. L.; Abresch, E. C.; Okamura, M. Y.; Yeh, A. P.; Rees, D. C.; Feher, G. J Mol Biol 2002, 319, 501.
9. Lange, C.; Hunte, C. Proc Natl Acad Sci USA 2002, 99, 2800.
10. Brooks, B. R.; Bruccoleri, R. E.; Olafson, B. D.; States, D. J.; Swaminathan, S.; Karplus, M. J Comp Chem 1983, 4, 187.
11. MacKerell, A. D.; Bashford, D.; Bellot, M.; Dunbrack, R. L.; Evansec, J. D.; Field, M. J.; Fisher, S.; Gao, J.; Guo, H.; Ha, S.; Joseph, D.; Kuchnir, L.; Kuczera, K. K.; Lau, F. T. K.; Mattos, C.; Michnick, S.; Ngo, T.; Nguyen, D. T.; Prodhom, B.; Reiher, I. W. E.; Roux, B.; Schlenkrich, M.; Smith, J.; Stote, R.; Straub, J.; Watanabe, M.; Wiorkiewicz–Kuczera, J.; Yin, D.; Karplus, M. J Phys Chem B 1998, 102, 3586.
12. Cornell, W. D.; Cieplak, P.; Bayly, C. I.; Gould, I. R., Jr.; Merz, K. M.; Ferguson, D. M.; Spellmeyer, D. C.; Fox, T.; Cladwell, J. W.; Kollmann, P. A. J Am Chem Soc 1995, 117, 5179.
13. Northrup, S. H.; Pear, M. R.; Morgan, J. D.; McCammon, J. A.; Karplus, M. J Mol Biol 1981, 153, 1087.
14. http://alta1.middlebury.edu/chemistry/software/heme/2003.
15. Rush, T. S.; Kozlowski, P. M.; Piffat, C. A.; Kumble, R.; Zgierski, M. Z.; Spiro, T. G. J Phys Chem B 2000, 104, 5020.
16. Rai, B. K.; Durbin, S. M.; Prohofsky, E. W.; Sage, J. T.; Ellison, M. K.; Roth, A.; Scheidt, W. R.; Sturhahn, W.; Alp, E. E. J Am Chem Soc 2003, 125, 6927.
17. Ceccarelli, M.; Procacci, P.; Marchi, M. J Comp Chem 2002, 24, 129.
18. Siegbahn, P. E. M. Q Rev Biophys 2003, 36, 91.
19. Mao, J.; Zhang, Y.; Oldfield, E. J Am Chem Soc 2002, 124, 13911.
20. Rovira, C.; Carloni, P.; Parrinello, M. J Phys Chem B 1999, 103, 7031.
21. Bayly, C. I.; Cieplak, P.; Cornell, W. D.; Kollman, P. A. J Phys Chem 1993, 97, 10269.
22. Kashiwagi, H.; Obara, S. Int J Quantum Chem 1981, 20, 843.
23. Spartan'02 Irvine, CA 2001.
24. Gaussian03 Carnegie, PA 2003.
25. Humphrey, W. F.; Dalke, A.; Schulten, K. J Mol Graph 1996, 14, 33.
26. Jorgensen, W. L.; Chandrasekhar, J.; Madura, J. D.; Impey, R. W.; Klein, M. L. J Chem Phys 1983, 79, 926.
27. Stewart, J. J. P. J Comp Chem 1989, 10, 209.
28. Besler, B. H. J Comp Chem 1990, 11, 431.
29. Kalé, L.; Skeel, R.; Bhandarkar, M.; Brunner, R.; Gursoy, A.; Krawetz, N.; Phillips, J.; Shinozaki, A.; Varadarajan, K.; Schulten, K. J Comput Phys 1999, 151, 283.
30. Rocchia, W.; Alexov, E.; Honig, B. J Phys Chem B 2001, 105, 6507.
31. Nicholls, A.; Sharp, K. A.; Honig, B. Proteins Struct Funct Genet 1991, 11, 281.
32. Read, J.; Gill, R.; Dales, S. L.; Cooper, J. B.; Wood, S. P.; Anthony, C. Protein Sci 1999, 8, 1032.
33. McGee, W. A.; Rosell, F. I.; Liggins, J. R.; Rodriguez–Ghidarpour, S.; Luo, Y.; Chen, J.; Brayer, G. D.; Mauk, A. G.; Nall, B. T. Biochemistry 1996, 35, 1995.
34. Nordgren, C. E.; Tobias, D. J.; Klein, M. L.; Blasie, J. K. Biophys J 2002, 83, 2906.